

RESEARCH PAPER

ESTIMATION OF TEMPERATURE CHANGE IN THE HUMAN BRAIN DURING MAGNETIC RESONANCE IMAGING PROCEDURE

Christiana Subaar¹, Joseph K. Amoako², Alfred Owusu³, Kwasi Preko¹ Sylvester Kojo Danuor¹

¹Department of Physics, Kwame Nkrumah University of Science and Technology, Kumasi, Ghana

²Radiation Protection Institute, Ghana Atomic Energy Commission (GAEC), Accra, Ghana

³Department of Physics, University of Cape Coast, Cape Coast, Ghana

*Corresponding author: ysubaar@gmail.com

ABSTRACT

The study measured brain (head) temperature variation of patients during magnetic resonance imaging (MRI) examinations. The challenges of measuring temperature increase in-vivo during MRI have led to an increase in the use of numerical methods to precisely predict and quantify the temperature increase and distribution in the human brain during a normal MRI scan. To this end, an explicit formula in the finite difference time domain has been applied to solve Penne's bioheat equation with the help of the matrix laboratory (MATLAB) programming language. Three-dimensional temperature distribution in patients during MRI was estimated. The study was carried out at the 37 Military Hospital and the Diagnostic Center Limited, Ghana. Fifty (50) adult patients' forehead temperatures were measured with an infra-red thermometer before and after the MRI. The ages of the patients ranged from 32 to 68 years, with a body mass index ranging between 22.16 and 44.16 kgm⁻². The lowest temperature during the MRI from the simulated results was 37.5 °C and the highest temperature was 42.5 °C. The results during MRI scan depicted brain hyperthermia, predicting that the radiofrequency of electromagnetic radiation during MRI leads to tissue heating resulting temperature being highest on the skin, low in the skull, and higher again in the brain. The highest stimulated brain temperature during the brain MRI study depicts brain hyperthermia, and this effect may be caused by the MRI components and the pathological condition of the patient. The experimental results validated the theoretical results by showing that there is a temperature increase after patients' brain MRI scans. However, the intermittently measured pre-and post-scan temperatures were all within guidance level of 1 °C recommended by the United States Food and Administration and the International Electrotechnical Commission.

Keywords: Hyperthermia; Patients; Finite difference time domain; radiofrequency

INTRODUCTION

Magnetic resonance imaging (MRI) has become a significant diagnostic procedure because of its high resolution since Paul Christian Lauterbur and Peter Mansfield in 1974 independently published a work which made the development of MRI possible (Kauffman, 2014). The use of this imaging technique has increased enormously in medical settings since it produces high-quality images of the internal structure of the human body and is considerably safer than x-ray or radio-isotope techniques. (Viscuse et al., 2015; ICNIRP, 2004).

The advance in clinical high-field static magnetic fields (B_0) for human is between 0.2 T and 3.0 T (Davies et al., 2015; Van, Matthias & Webb, 2014). During magnetic resonance imaging, patients are placed in an MRI scanner with inbuilt components, which consist of static magnetic fields, faster, and stronger gradient magnetic fields, and more powerful radiofrequency (RF) transmission coils (Durbidge, 2011; Jagannathan, 1999). Also, the coils of the MRI magnet are encased in a thermos-bottle-like housing to minimise heat leaking into the innermost part of the magnet. The dangers confronted in MRI emerge primarily from these components: the physiological monitoring device and the skin contact with the monitoring sensor or RF coil cable during the imaging process (Bashein & Syrov, 1991; Brown, Goldstein, & Little, 1993; Hall, Stevenson, & Suresh, 1992; Hartwig et al., 2009; Jones et al., 1996; Keens & Laurence, 1996).

The radiofrequency (10 to 400 MHz) of the magnetic field (B_1) in the MRI excites the patient's protons within B_0 , causing the emission of a signal used in the formation of the magnetic resonance images. Gradient magnetic fields (dB/dt) localise the aligned protons caused by the net magnetization generated by B_0 inside the body for spatial reconstruction of tissue into images (BCCDC,

2013). The magnitude of B_1 through the RF coil depends on the magnet field strength that surrounds the patient inside the magnet bore (Chen & Steckner, 2017).

The temperature increase during MRI is as a result of RF exposures and it is more directly related to potential hazards which may include painful sensation (Hardy, Wolff & Goodell, 1967). Conventional temperature monitoring equipment and thermometers were not designed to operate in the harsh MRI environment that utilises electromagnetic fields (EMFs) that can adversely affect or alter the operation of MRI. Measuring brain temperature increase in-vivo during MRI is very invasive, and remote measuring techniques are blunt and often inaccurate (Stauffer et al., 2014; Shellock, 2011).

Despite the acceptable ambient MRI environment, the cause of profuse localised sweating of some patients during MRI has not yet been reported, though some potential hazards of RF electromagnetic fields (EMF) have been reported. Studies have been conducted on brain temperature changes immediately before and after an MRI exposure of the brain (Dery et al., 2013; Shellock & Crues, 1988; Subaar et al., 2017) and the effect of temperature immediately after brain MRI on body core temperature (Machata et al., 2009). None of the studies examine real-time measurement of temperature changes during brain MRI exposure. However, some theoretical models suggest that there is an excessive increase in temperature during MRI exposures with the highest elevation localised at the forehead during brain MRI (Subaar et al., 2017). It is relevant to monitor the patient's temperature during an MRI scan to avoid hyperthermia, which can cause harm by increasing body temperature and damaging biological organs and tissues. The current produced by the RF pulses has the potential to induce localised burns (Wang et al., 2007), especially if a body part is

touching the RF coil cable. Therefore, this paper computationally modelled temperature distribution of patients head before and during MRI scan. The numerical result was compared with the experimental patients' measured temperatures before and after brain MRI exposures of frequencies above 100 kHz for a total examination scans with time less than an hour. The number of people exposed to the RF field of the electromagnetic field from a diagnostic MRI in Ghana has increased over the last decade (Piersson & Gorleku, 2017; Opoku et al., 2013). There is, therefore, the need to numerically predict temperature distribution to create awareness of the potential hazards caused by diagnostic MRI exposures, especially in research settings since a 2.5 T field strength currently in Ghana can cause appreciable thermal effects.

MATERIALS AND METHODS

A three-dimensional (3-D) Bio-Heat Equation (BHE) was modelled using the MATLAB programming language, evaluating the effects of RF radiation exposure in the human head and also determining the induced internal EMF and its spatial distribution during brain MRI. The algorithm for the solved equation was stimulated to demonstrate the thermal interaction of the biological tissue in the brain. The numerical results were compared with patients' (head) brain temperatures measured before and after MRI operating above 100 kHz.

Theoretical Analysis: Temperature Variation

Temperature increase analysis of EMF of RF power deposition during brain MRI examinations was simulated. An explicit method based on finite difference time domain (FDTD) was applied to solve Penne's Bio-Heat (PBH) equation (1948) to determine the temperature change in the human tissue during brain MRI. In this paper, the central difference scheme of FDTD was employed to discretize the heat equation and assume time is dependent. MATLAB version R2017A was used to write algorithms for the solved equations and was stimulated to demonstrate the induced EMF and its spatial distribution during brain MRI as well as the thermo-mechanical interaction of the biological tissue.

A physical model of the research shown in Figure 1 depicted the temperature distribution in the brain during brain MRI. Thermal properties for the biological tissues contained in the human head model, which were taken to be constant, are shown in Table 1.

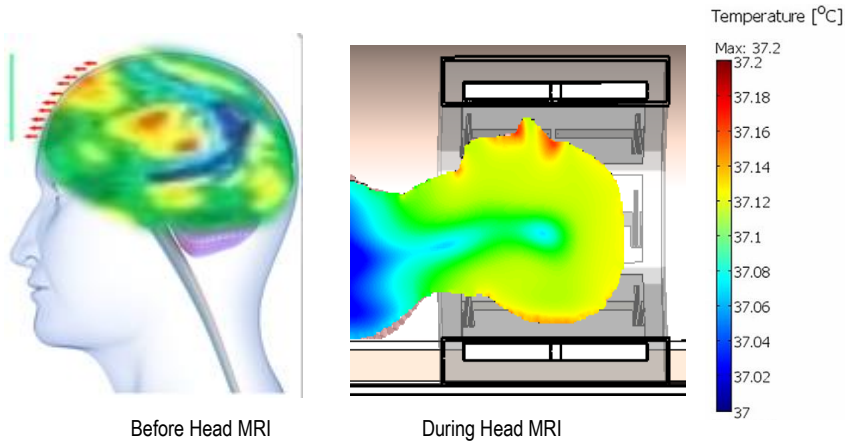


Figure 1: Physical model of homogeneous head temperature in 3-D

Source: (Wessapan, Srisawatdhisukul, & Rattanadecho 2012).

Table 1: Thermal properties for the biological tissues contained in the human head model (Collins et al., 2004)

Tissue	Density [kg/m ³]	Specific heat capacity [Jkg ⁻¹ °C ⁻¹]	Thermal conductivity [Wm ⁻¹ °C ⁻¹]	Volumetric heat generation rate [W/m ³]
Bone	1,080.0	2,110	0.650	26.1
Cerebrospinal Fluid	1,007.0	3,800	0.500	0.0
Gray Matter	1,035.5	3,680	0.565	15,575.0
White Matter	1,027.4	3,600	0.503	5.2
Muscle	1,041.0	3,720	0.498	687.0
Skin	1,100.0	3,150	0.342	1,100.0

The evolution and the distribution of the temperature inside the living tissues are governed by the heat-exchange such as the heat conduction, the blood flow and the metabolism. They also depend on the contribution of external sources, such as the power deposited by RF sources (Ozen, Helhel, & Bilgin, 2011). The partial differential equation of the Pennes Bio-Heat (PBH) equation is shown in Equation 1 (Pennes, 1948):

$$\rho C \frac{\partial T}{\partial t} = k \nabla^2 T + h_m + h_b \tag{1}$$

is given by Equation (2) as the 3-D expression of the PBH equation in the media with uniform material properties.

$$\rho_{(x,y,z)} c_{p(x,y,z)} \frac{\partial T_{(x,y,z)}}{\partial t} = k \frac{\partial^2 T}{\partial x^2} + k \frac{\partial^2 T}{\partial y^2} + k \frac{\partial^2 T}{\partial z^2} + w_b c_b (T_{(x,y,z,t)} - T_a) + Q_m(x,y,z) + Q_r(x,y,z,t) \cdot SAR - (hr_{(x,y,z)} + hc_{(x,y,z)} + he_{(x,y,z)}) \quad (2)$$

$T(x,y,z,t)$ is the instantaneous temperature of the tissue ($^{\circ}\text{C}$) at the point (x, y, z) and at the time, t . ρ is the density of tissue in kgm^{-3} , k is thermal conductivity of tissue in $\text{Wm}^{-1}\text{C}^{-1}$, c is tissue specific heat in $\text{J kg}^{-1}\text{C}^{-1}$, Q_r is the regional heat source in $\text{W}\backslash\text{m}^3$, Q_m is the metabolic heat generation rate in $\text{W}\backslash\text{m}^3$, w_b is blood perfusion rate in $\text{kg}\backslash(\text{m}^3 \text{ s})$, c_b is the blood specific heat, T_a is the arterial temperature and $(T_{(x,y,z,t)} - T_a)$ is temperature change of patients in $^{\circ}\text{C}$, $\frac{\partial T_{(x,y,z)}}{\partial t}$ is the temperature rise rate. The main assumption of this model is that blood enters the brain with the body temperature and leaves it with the brain temperature. For the transient head temperature distribution, the air temperature with time-varying movement inside the spherical head and the heat dissipated by the time-dependent convection, $k \frac{\partial T}{\partial A} = h(t)(T - T_{art})$ where T_{en} is the environmental temperature and h is the heat transfer coefficient. $T(A) = T_o(A)$, when $t=0$. The study analysed the rise in temperature associated with the exposure to MRI RF emissions. In this case, the expected rise in temperature is small. Therefore, it is also assumed that the electromagnetic dielectric and thermal properties of the biological tissues are not modified by such a small increase in temperature.

The maximum raise in temperature (δT_{max}) caused by the electromagnetic energy deposited was obtained from the difference between the temperature for the exposed model to RF emissions with Specific Absorption Rate (SAR), ($\text{SAR} \neq 0$) and that of the unexposed model ($\text{SAR} = 0$) (with the patients set in head coil inside MRI scanner yet to be scanned).

Numerical Model of Penne's Bio-Heat Equation

In the finite difference time domain, the rise in temperature is the difference between the temperature calculated for the model exposed to the RF source, $T[(i,j,k,t), (\text{SAR} \neq 0)]$, and $T[(i,j,k,t), (\text{SAR} = 0)]$, which is the temperature for the unexposed model. The Explicit Method is derived through a differential approach by the discretization of the PBH equation on an orthogonal grid for a uniform spacing by applying a finite difference scheme. With this approach, at the location $(i\delta x, j\delta y, k\delta z)$, the temperature at time step $n + 1$ is estimated using the thermal properties of biological tissues shown in Table 1 and the temperature at time step n .

Approximation of time derivatives

In order to solve Equation 2, the time grid, $0 = t_0 < t_1 < \dots < t_{f-2} < t_{f-1} < t_f < \dots < t_F < \infty$ with constant step, $\Delta t = t_f - t_{f-1}$ is introduced using Lagrange interpolations. For the points $(t_{f-2}, T_{f-2}), (t_{f-1}, T_{f-1})$ & (t_f, T_f) ,

where $T_{f-2} = T(x, y, z, t_{f-2}), T_{f-1} = T(x, y, z, t_{f-1}), T_f = T(x, y, z, t_f)$ are obtain and expressed as Equation (3).

$$t \in [t_{f-2}, t_f]: T(x, y, z, t) = T_{f-2} \frac{(t-t_{f-1})(t-t_f)}{(t_{f-2}-t_{f-1})(t_{f-2}-t_f)} + T_{f-1} \frac{(t-t_{f-2})(t-t_f)}{(t_{f-1}-t_{f-2})(t_{f-1}-t_f)} + T_f \frac{(t-t_{f-2})(t-t_{f-1})}{(t_f-t_{f-2})(t_f-t_{f-1})}$$

$$= T_{f-2} \frac{(t-t_{f-1})(t-t_f)}{2(\Delta t)^2} - T_{f-1} \frac{(t-t_{f-2})(t-t_f)}{(\Delta t)^2} + T_f \frac{(t-t_{f-2})(t-t_{f-1})}{2(\Delta t)^2} \tag{3}$$

On the basis of Equation 3 the time derivative is calculated as Equation 4:

$$t \in [t_{f-2}, t_f]: \frac{\partial T(x, y, z, t)}{\partial t} = T_{f-2} \frac{2t-t_f-t_{f-1}}{2(\Delta t)^2} - T_{f-1} \frac{2t-t_f-t_{f-2}}{(\Delta t)^2} + T_f \frac{2t-t_{f-1}-t_{f-2}}{2(\Delta t)^2} \tag{4}$$

and then,

$$\left. \frac{\partial T(x, y, z, t)}{\partial t} \right|_{t=t_f} = \frac{T_{f-2} - 4T_{f-1} + 3T_f}{2\Delta t}$$

Finite Difference Time Domain (FDTD)

A 3-D Problem and domain oriented in the Cartesian coordinate system (x, y, z) generates Equation (5).

$$\nabla^2 T(x, y, z) = \frac{\partial^2 T(x, y, z, t)}{\partial x^2} + \frac{\partial^2 T(x, y, z, t)}{\partial y^2} + \frac{\partial^2 T(x, y, z, t)}{\partial z^2} \tag{5}$$

Applying the central difference scheme to Equation 5 with respect to the geometrical coordinates to a constant mesh step, h, Equation 5 becomes

$$\left(\frac{\partial^2 T}{\partial x^2} + \frac{\partial^2 T}{\partial y^2} + \frac{\partial^2 T}{\partial z^2} \right) = \frac{T_{i-1,j,k} - 2T_{i,j,k} + T_{i+1,j,k}}{h^2} + \frac{T_{i,j-1,k} - 2T_{i,j,k} + T_{i,j+1,k}}{h^2} + \frac{T_{i,j,k-1} - 2T_{i,j,k} + T_{i,j,k+1}}{h^2} \tag{6}$$

where $T_{i,j,k} = T(x_i, y_j, z_k, t), T_{i-1,j,k} = T(x_{i-1}, y_j, z_k, t)$ and so on

Using the explicit scheme of FDTD, Equation (1) is approximated as Equation 7.

$$\frac{\rho C_p}{2k\Delta t} (T_{i,j,k}^{(f-2)} - 4T_{i,j,k}^{(f-1)} + 3T_{i,j,k}^{(f)}) = \frac{1}{h^2} (T_{i-1,j,k}^{f-1} + T_{i+1,j,k}^{f-1} + T_{i,j-1,k}^{f-1} + T_{i,j+1,k}^{f-1} + T_{i,j,k-1}^{f-1} + T_{i,j,k+1}^{f-1} - 6T_{i,j,k}^{f-1})$$

$$+ \frac{w_b c_b}{k} (T_a - T_{i,j,k}^{(f-1)}) + \frac{Q_m}{k} \tag{7}$$

Equation7 generates a system of linear equations as shown in Equation 8

$$3 \left\{ \frac{\rho C_p}{2k\Delta t} \right\} T_{i,j,k}^{(f)} = \left\{ \frac{4\rho C_p}{2k\Delta t} - \frac{w_b c_b}{k} - \frac{6}{h^2} \right\} T_{i,j,k}^{(f-1)}$$

$$+ \frac{1}{h^2} \left(T_{i-1,j,k}^{f-1} + T_{i+1,j,k}^{f-1} + T_{i,j-1,k}^{f-1} + T_{i,j+1,k}^{f-1} + T_{i,j,k-1}^{f-1} + T_{i,j,k+1}^{f-1} - \frac{\rho C_p}{2k\Delta t} T_{i,j,k}^{(f-2)} + \frac{w_b c_b T_a + Q_m}{k} \right) \tag{8}$$

Estimation of Temperature Change in the Human Brain

The resultant linear Equation 8 was solved with a programming language (MATLAB version, R2017A). The algorithms for the solved equations were stimulated to demonstrate the thermo-mechanical interaction of the biological tissue in the brain.

Experimental procedure

Consent from patients and/or their legal representatives for participation in the study was received after the study protocol was approved by the University of Cape Coast Review Board (UCCIRB) with ethical clearance – ID NO: (UCCIRB/CHAS/2016/01).

Fifty (50) adult patients aged 32 to 68 years, with a body mass index ranging from 22 to 45 kgm^{-2} were exposed to diagnostic brain MRI at 0.3 T and 1.5 T with operating frequencies above 100 kHz. The measurements were taken at two centres, the 37 Military Hospital, Accra, which uses a 1.5 T superconducting magnetic machine of Philips Magnetic Resonance Systems Achieve, Release 2.6 level 12008-07-11-CE 0344 with model number 43000-574 and serial number 707703, and the Diagnostic Centre Limited,

Accra, which uses a 0.3 T permanent magnet machine of an Airis Elite version V5.1H manufactured by Hitachi Medical Corporation of Japan and product classification of II-a. An infra-red thermometer calibrated at the temperature laboratory of the Ghana Standards Authority, Accra-Ghana (accuracy $0.1^{\circ}\text{C} / 33.8^{\circ}\text{F}$) was used to measure pre-and-post scan tympanic temperatures of patients by inserting it into their right ear canals. Patients' temperatures were measured once immediately before and after MRI scan. The total scan duration (which was in the region of 22 to 32 minutes) and the temperature changes during brain scans for fifty patients were recorded. Data analysis was performed with the help of the Python 3.8 version.

RESULTS - Numerical Results

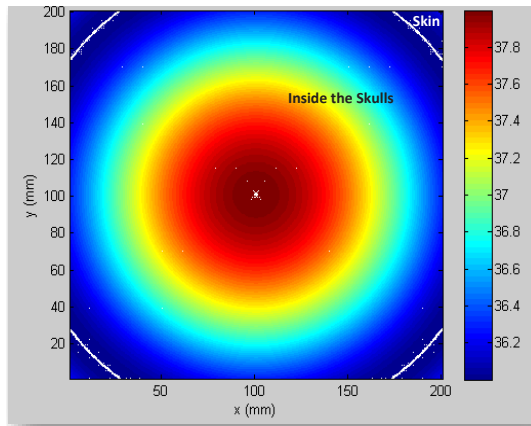


Figure 2: 2-D Anticipated Brain temperature before brain MRI exposure

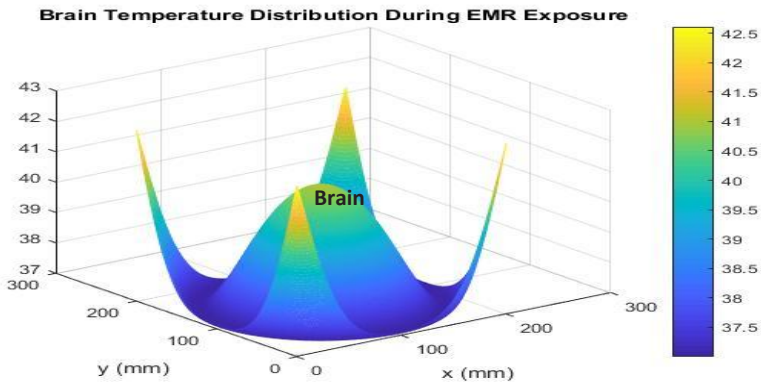


Figure 3: 3-D Anticipated Brain Temperature during Brain MRI exposure

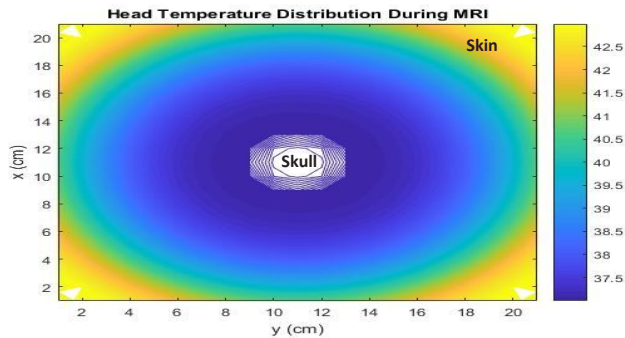


Figure 4: 2-D Anticipated head temperature during brain MRI exposure

Estimation of Temperature Change in the Human Brain

The thermal simulation of electromagnetic RF of frequencies above 100 kHz based on the FDTD method depicted temperature changes caused by RF absorption during brain MRI using 2-D and 3-D BHE, as illustrated in Figures 2, 3 and 4. Figure 2 shows the patient's temperature before the MRI scan. The peak temperature changes caused by the

electromagnetic RF absorption in Figure 3 are illustrated by a 2-D picture shown in Figure 4 as the hot spots during an MRI scan. The 3-D simulation depicted volumetric energy deposition due to RF absorption during an MRI scan. The RF fields emitted during the MRI penetrated the exposed biological tissues and produced heat, as shown in Figure 3.

Experimental Results

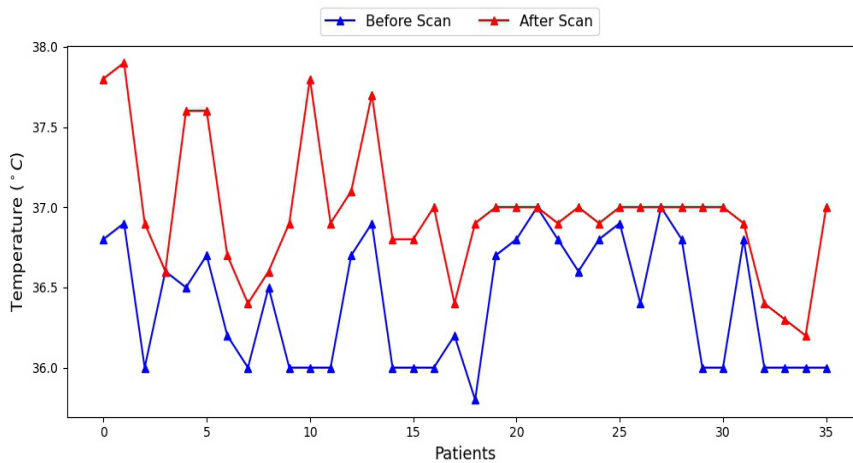


Figure 5: Pre-and-Post MRI brain temperatures of the thirty-six patients at 1.5 T

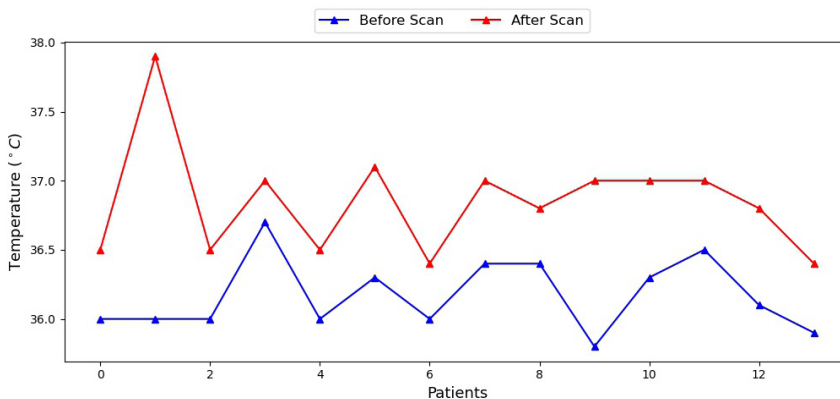


Figure 6: Pre- and Post-MRI brain temperatures of the fourteen patients at 0.3 T.

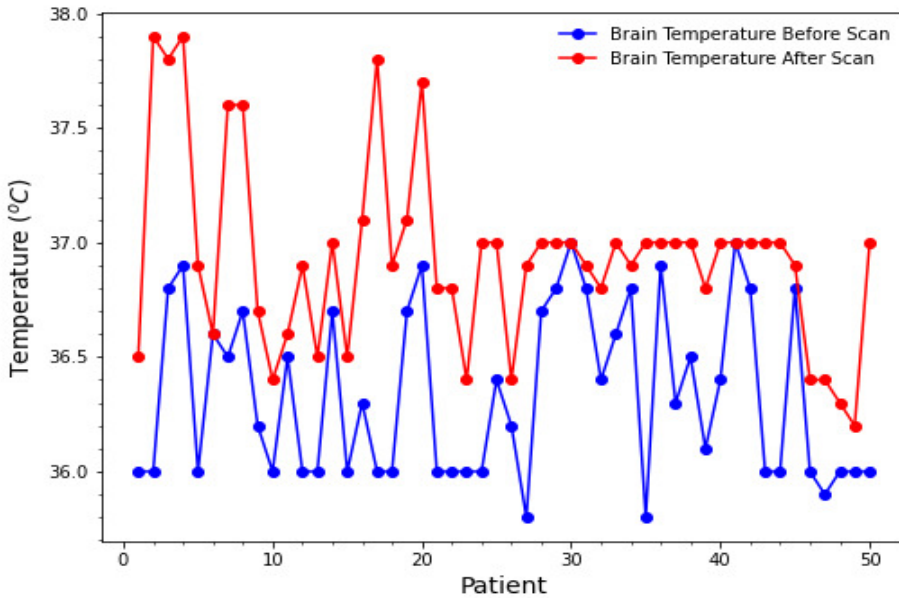


Figure 7: Pre- and Post-MRI brain temperatures of the fifty patients.

The experimental study was conducted at the MRI facilities at field strengths of 0.3 T and 1.5 T to provide additional validation of the numerical model. The patient’s pre-and post-MRI scan temperatures were recorded using an infra-red thermometer. Figure 5, 6 and 7 show brain temperatures recorded before and after MRI scans of the fifty (50) patients aged from 32-68 years for brain MRI exposures at RF above 100 kHz at field strengths of 1.5 T and 0.3 T.

DISCUSSION

The simulated results include contributions from environmental parameters as well as radiation, convection, and evaporation. The results, therefore, indicated anticipating thermal effects during the head MRI. This thermal effect include hyperthermia and tissue damage. The minimum temperature recorded during the MRI was 0.5°C higher than the baseline physiological temperature, which was

37.5 °C. The highest temperature measured at skin was 42.5°C. This maximum temperature recorded was within the temperature upper limit at which painful sensations or damage occur (Hardy et al., 1967). Due to the different thermal properties of the tissues and the organs of the head, Figure 3 showed that the RF of the electromagnetic radiation of MRI, which leads to tissue heating, was at its highest in the skin, low in the skull, but higher again in the brain, and this agrees with Leeuwen et al., (Van Leeuwen et al.,1999).

According to the study conducted in 2004, it is not surprising that the maximum SAR of the RF causing the hyperthermia was within the skin, which indicated “hot spots” sites since the magnitude of the electric field from the RF transmitter to the tissue increased dramatically as one approached the transmitter coil. The results agree with the findings of Nguyen et al., 2004 and Zamanian & Hardiman, 2005 that there is

Estimation of Temperature Change in the Human Brain

a low penetration of RF electromagnetic energy at the skin surface, leading to the high absorption of RF energy. This accounts for the hot spots of the skin region, as clearly shown in Figure 4, and can lead to burning effects. The simulated results showed that during a brain MRI exposure, an abnormally high brain temperature is possible. This paper, therefore, indicated that the hyperthermia recorded in this study may affect the body's regulatory mechanism.

Based on the United States Food and Drug Administration (USFDA) and the International Electrotechnical Commission recommendations, the maximum core temperature increase should not exceed 1.0 °C and the maximum temperature in the head should not reach 38 °C (Ng, 2003; Zaremb & Phillips, 2002; IEC, 2001). The simulated results showed that the average temperature during a brain MRI exposure of frequencies above 100 kHz exceeded the FDA recommendation. However, the thermal model presented does not account for all thermal regulation responses of the body and thus represents a worst-case scenario.

During the experimental study the temperatures measured before and after brain MRI of patients with an infra-red thermometer at both MRI facilities (0.3 T and 1.5 T) were in the range of 35.8 oC–37.9 oC at a scan duration of 30 minutes, in spite of keeping the ambient temperature of the MRI suite at 20–24 oC with no active warming device being used. By comparing the numerical results with the experimental results, the measured brain temperatures were measured intermittently by measuring the right tympanic temperature before and after the brain MRI with infra-red thermometer. This therefore accounted for the difference in the magnitude of the temperature values in both the numerical and experimental results as shown in Figures 2, 3 and 4.

The temperature before the scan was in the range of 35.8 oC to 37 oC and that after the scan was in the range of 36.2 oC to 37.9 oC as shown in Figure 7. The experimental results of temperature before and after the scan indicated an increase in brain temperature after brain MRI, although the recorded post-scan temperatures were all within guidance levels since the rise in temperature was not more than 1.0 oC (Ng, 2003). Hence, the brain temperatures of patients could be elevated above the guidance level during brain MRI exposures.

DELIMITATION

This study covered only fifty (50) adult patients who were referred for brain (head) MRI scans of frequency above 100 kHz. A three dimensional (3D) numerical model was developed from Penne's classical bio-heat equation to predict temperature distribution in patients undergoing brain MRI examinations. An explicit formula of finite difference time domain of Penne's classical bio-heat equation was developed. The central difference was employed to discretize the heat equations developed whilst Lagrange interpolation scheme was used to model the time independence equations assuming that the biological tissues of the human brain are homogeneous. The resultant linear equations were solved with a programming language (MATLAB version, R2017A).

LIMITATION

According to Nepa, 2012 in electromagnetic radiations and biological interactions, the magnetically induced field component of the electromagnetic field is size dependent, while the electric coupling is independent of size (Faruque, Islam, & Misran, 2010). The temperature distributions along the three dimensions of the head (brain) are size independent. The experimental data were collected from MRI of field strength of 0.3

T and 1.5 T. The body parts excluded in the study include abdomen and pelvis, joints, and Spine. Due to the high cost of MRI scan examination only fifty (50) adult patients underwent head (brain) MRI examination in the period of 12 months of field strength of 0.3 T recording fourteen (14) patients and 1.5 T recording thirty-six (36) patients. The physical parameters of the biological tissues (Table 1) that approximate heterogeneous head (brain) structure of a human being were used in the study, but the solved equations simulated RF EMF of frequency above 100 kHz of homogeneous tissue inside human brain depicting temperature changes within brain which vary by depth depicting the heterogeneous nature of head.

CONCLUSION

The numerical study of RF exposure suggested that the majority of RF pulses used in MRI for the excitation of the nuclei were transformed into heat within the patient's tissue. The lowest temperature during MRI from the simulated results was 37.5°C and the highest temperature was 42.5°C. The numerical study has to some extent showed that the tissues and the organs of the head have different thermal properties as shown in Table 1 despite the fact that the study assumed that the biological tissues of the human brain are homogeneous. The experimental results validated the theoretical results by showing that there is a temperature increase after patients' brain MRI scans. However, the intermittently measured pre-and post-scan temperatures were all within guidance levels. The study therefore predicted that there is excessive elevation of patients' brain temperatures during brain MRI, which could exceed the guidance level. With the appropriate boundary conditions and non-invasive monitoring of patient temperature during brain MRI, temperature change in the brain was simulated. However, in terms of safety, it is desirable to monitor

patients' temperature in the MRI environment since absorption of energy from RF fields of electromagnetic radiation by tissues results in the generation of heat due to resistive losses of tissue.

ACKNOWLEDGEMENT

The study was fully sponsored by the Ghana Education Trust Fund (GetFUND). 37-Military hospital and the Diagnostic Center Limited are acknowledged for allowing the use of their MRI facilities.

REFERENCES

- British Columbia Centre for Disease Control (BCCDC), (2013). Radiofrequency Toolkit for Environmental Health Practitioners.
- Bashein, G., & Syrový, G. (1991). Burns associated with pulse oximetry during magnetic resonance imaging. *Anesthesiology: The Journal of the American Society of Anesthesiologists*, 75(2), 382-382.
- Brown, T. R., Goldstein, B., & Little, J. (1993). Severe burns resulting from magnetic resonance imaging with cardiopulmonary monitoring. Risks and relevant safety precautions. *American journal of physical medicine & rehabilitation*, 72(3), 166-167.
- Chen, X., & Steckner, M. (2017). Electromagnetic computation and modeling in MRI. *Medical Physics*, 44(3), 1186-1203.
- Collins, C. M., Liu, W., Wang, J., Gruetter, R., Vaughan, J. T., Ugurbil, K., & Smith, M. B. (2004). Temperature and SAR calculations for a human head within volume and surface coils at 64 and 300 MHz. *Journal of Magnetic Resonance Imaging*, 19(5), 650-656.
- Davies G. R., Broche L. M., Pine K. J., Ross P. J., & Lurie D. J. (2015). In vivo human brain

Estimation of Temperature Change in the Human Brain

- imaging at 0.2 T using a whole-body fast field-cycling MRI system.
- Dery, T. B., Darko, E. O., Amoako, J. K., & Kyere, A. K. (2013). An Iterative Method for the Determination of Temperature Distribution in Patients Undergoing Brain Magnetic Resonance Imaging (MRI) Examinations. *International Journal of Science and Technology*, 3(3).
- Durbridge, G. (2011). Magnetic resonance imaging: fundamental safety issues. *journal of orthopaedic & sports physical therapy*, 41(11), 820-828.
- Faruque, M. R. I., Islam, M. T., & Misran, N. (2010). Effect of human head shapes for mobile phone exposure on electromagnetic absorption. *Informacije MIDEM*, 40(3), 232-237.
- Hall S. C., Stevenson G. W., & Suresh S. (1992). Burn associated with temperature monitoring during magnetic resonance imaging. *The Journal of the American Society of Anesthesiologists*, 76(1), 152-152.
- Hardy, J. D., Wolff, H. G., & Goodell, H. (1967). Pain sensations and reactions. Williams and Wilkins, 1952: reprinted by Hafner Publishing Co, New York.
- Hartwig, V., Giovannetti, G., Vanello, N., Lombardi, M., Landini, L., & Simi, S. (2009). Biological effects and safety in magnetic resonance imaging: a review. *International Journal of Environmental Research and Public Health*, 6(6), 1778-1798.
- International Electrotechnical Commission (IEC). (2001). Particular Requirement for the Safety of Magnetic Resonance Equipment for Medical Diagnosis, Medical electrical equipment, IEC 60601-2-33.
- Jagannathan, N. R. (1999). Magnetic resonance imaging: bioeffects and safety concerns. *Indian Journal of Biochem Biophys*, 36(5), 341-7.
- Jones, S., Jaffe, W., & Alvi, R. (1996). Burns associated with electrocardiographic monitoring during magnetic resonance imaging. *Burns*, 22(5), 420-421.
- Kauffman, G. (2014). Nobel prize for MRI imaging denied to Raymond V. Damadian a decade ago. *Chemical Educator*, 19, 73-90.
- Keens S. J., & Laurence A. S. (1996). Burns caused by ECG monitoring during MRI imaging. *Anaesthesia*, 51(12), 1188-1189.
- Machata, A. M., Willschke, H., Kabon, B., Prayer, D., & Marhofer, P. (2009). Effect of brain magnetic resonance imaging on body core temperature in sedated infants and children. *British journal of anaesthesia*, 102(3), 385-389.
- Nepa, P. (2012). Electromagnetic Radiations and Biological Interactions. Retrieved 28/01/2016, 2016, from p. nepa@iet.unipi.
- Ng, K. H. (2003). Non-ionizing Radiations—Sources, Biological Effects, Emissions and Exposures. Paper presented at the Proceedings of the international conference on non-ionizing radiation at UNITEN.
- Nguyen, U. D., Brown, J. S., Chang, I. A., Krycia, J., & Mirotznik, M. S. (2004). Numerical evaluation of heating of the human head due to magnetic resonance imaging. *IEEE Transactions on Biomedical Engineering*, 51(8), 1301-1309.
- Opoku, S., Antwi, W., & Sarblah, S. R. (2013). Assessment of safety standards of magnetic resonance imaging at the Korle Bu Teaching Hospital (KBTH) in Accra, Ghana. *Imaging and Radioanalytical Techniques in Interdisciplinary Research—Fundamentals and Cutting-Edge Applications*.

- Ozen, S., Helhel, S., & Bilgin, S. (2011). Temperature and burn injury prediction of human skin exposed to microwaves: a model analysis. *Radiation and environmental biophysics*, 50(3), 483-489.
- Pennes, H. H. (1948). Analysis of tissue and arterial blood temperatures in the resting human forearm. *Journal of Applied Physiology*, 1(2), 93-122.
- Piersson, A. D., & Gorleku, P. N. (2017). Assessment of availability, accessibility, and affordability of magnetic resonance imaging services in Ghana. *Radiography*, 23(4), e75-e79.
- International Commission on Non-Ionizing Radiation Protection (ICNIRP). (2004). Medical magnetic resonance (MR) procedures: protection of patients. *Health Physics*, 87(2), 197-216. .
- Shellock, F. G. (2011) MRI Safety: Monitoring Body Temperature During MRI Retrieved from <https://www.diagnosticimaging.com/view/mri-safety-monitoring-body-temperature-during-mri>
- Shellock, F. G., & Crues, J. V. (1988). Temperature changes caused by MR imaging of the brain with a head coil. *American journal of neuroradiology*, 9(2), 287-291.
- Stauffer P. R., Snow B. W., Rodrigues D. B., Salahi S., Oliveira T. R., Reudink D., & Maccarini P. F. (2014). Non-Invasive Measurement of Brain Temperature with Microwave Radiometry: Demonstration in a Head Phantom and Clinical Case. *The Neuroradiology Journal* 27: 3-12, 2014
- Subaar C., Amoako J. K., Owusu A., Fletcher, J. J., & Suurbaar, J. (2017). Numerical studies of adiofrequency of the electromagnetic radiation power absorption in paediatrics undergoing brain magnetic resonance imaging. *Journal of Radiation Research and Applied Sciences*.
- Van Leeuwen, G. M., Legendijk, J. W., Van Leersum, B. J., Zwamborn, A. P. M., Hornsleth, S. N., & Kotte, A. N. (1999). Calculation of change in brain temperatures due to exposure to a mobile phone. *Physics in medicine and biology*, 44(10), 2367.
- Van O., Matthias J. P., & Webb, A. G. (2014). Safety of ultra-high field MRI: what are the specific risks? *Current Radiology Reports*, 2(8), 61.
- Viscuse, P. V., Khasawneh, M., & Constantinou, C. (2015). MRI-Induced Second and Third Degree Burns to Hands Bilaterally: A Case Report. *Ann Hematol Oncol*, 2(7), 1053.
- Wang Z., Lin J. C., Mao W., Liu W., Smith, M. B., & Collins, C. M. (2007). SAR and temperature: simulations and comparison to regulatory limits for MRI. *Journal of Magnetic Resonance Imaging*, 26(2), 437-441.
- Wessapan, T., Srisawatdhisukul, S., & Rattanadecho, P. (2012). Specific absorption rate and temperature distributions in human head subjected to mobile phone radiation at different frequencies. *International Journal of Heat and Mass Transfer*, 55(1), 347-359.
- Zamanian, A., & Hardiman, C. (2005). Electromagnetic radiation and human health: A review of sources and effects. *High Frequency Electronics*, 4(3), 16-26.
- Zaremba, L., & Phillips, R. (2002). FDA guidelines for magnetic resonance equipment safety. Paper presented at the MEDICAL PHYSICS.